

Role of $\Sigma^*(1/2^-)$ baryons in $\Lambda_c \rightarrow \Lambda\pi^+\pi^+\pi^-$ decay

Jun He*

School of Physics and Technology, Nanjing Normal University, Nanjing 210097, China

(Dated: July 11, 2025)

Based on Belle data, the structure around 1435 MeV and the role of the $\Sigma(1380)$ resonance in the decay process $\Lambda_c \rightarrow \Lambda\pi^-\pi^+\pi^+$ are investigated. The $\Lambda\pi^\pm$ invariant mass spectra are approximately reproduced by the contribution from the $\Sigma(1385)$, modeled as a Breit-Wigner resonance combined with background. However, an additional contribution is required to account for the pronounced enhancement near 1435 MeV. To describe this structure, two scenarios are considered for the $\Sigma(1435)$: one as a Breit-Wigner resonance with spin-parity $1/2^-$ described via effective Lagrangians, and the other as a rescattering effect arising from coupled-channel interactions. Specifically, the channels $\bar{K}^0 p$, $\pi^0\Sigma^+$, $\pi^+\Sigma^0$, $\pi^+\Lambda$, and $\eta\Sigma^+$ are included for the positively charged mode, and K^-n , $\pi^0\Sigma^-$, $\pi^-\Sigma^0$, $\pi^-\Lambda$, and $\eta\Sigma^-$ for the negatively charged mode. The rescattering contributions are evaluated using the quasipotential Bethe-Salpeter equation approach. Simulated invariant mass spectra are generated and fitted to the experimental data. Both the Breit-Wigner and rescattering mechanisms provide reasonable descriptions of the enhancement near 1435 MeV. The rescattering approach naturally generates a cusp-like structure near threshold, which closely resembles the feature observed in the data. Furthermore, the inclusion of the $\Sigma(1380)$ resonance with spin-parity $1/2^-$ significantly improves the fit in the low-energy region and further enhances the description near 1435 MeV through interference effects. These results underscore the essential roles of the two $\Sigma^*(1/2^-)$ states in accurately describing the invariant mass distributions in the decay $\Lambda_c \rightarrow \Lambda\pi^+\pi^+\pi^-$.

I. INTRODUCTION

Light baryon resonances provide a crucial window into the nonperturbative regime of quantum chromodynamics, as their masses, decay patterns, and production mechanisms encode the underlying dynamics of strong interactions. Thanks to advances in accelerator and detector technologies, a wealth of high-precision data has been accumulated from facilities such as JLab and J-PARC, leading to an increasingly complete mapping of the nucleon and Δ resonance spectra. In contrast, hyperon spectroscopy remains far less explored: although Σ resonances were first reported in the 1960s, the Review of Particle Physics (PDG) currently lists only nine firmly established states (three- or four-star ratings), despite lattice QCD calculations and quark model predictions suggesting the existence of approximately 70 such states [1, 2]. Consequently, significant experimental and theoretical efforts have been devoted in recent years to advancing our understanding of hyperon spectrum.

In recent years, Σ resonances with spin-parity $1/2^-$ have attracted considerable attention. Within the framework of the constituent quark model, the lowest $\Sigma(1/2^-)$ state is predicted to have a mass around 1630 MeV [2]. Analyses of K^- -induced reaction data suggest the observation of a resonance $\Sigma(1620)$, potentially corresponding to this predicted state [3]. However, this resonance is currently rated as a one-star state by PDG, reflecting a low level of experimental confirmation [1]. Interestingly, several theoretical studies have predicted the existence of lower-mass $\Sigma(1/2^-)$ states, and experimental signals consistent with such states have also been reported, further stimulating interest and ongoing investigation in this sector [4, 5].

A $\Sigma(1/2^-)$ state around 1380 MeV has been theoretically predicted and supported by several experimental analyses. In the diquark model proposed by Jaffe and Wilczek, a $\Sigma(1/2^-)$ resonance near 1360 MeV was suggested [6]. Wu et al. found evidence for a new $\Sigma(1/2^-)$ resonance in the $K^-p \rightarrow \Lambda\pi^+\pi^-$ reaction, characterized by a broader width than the well-known $\Sigma(1385)$ with spin-parity $3/2^-$ [7–9]. Reference [10] demonstrated that the near-threshold enhancement in the $\pi^0\Lambda$ invariant mass spectrum of $\Lambda p \rightarrow \Lambda p\pi^0$ can be well described by including this $\Sigma(1/2^-)$ state. Further support for its existence comes from additional theoretical and experimental studies, including photoproduction $\gamma N \rightarrow K^+\pi\Lambda$, K^-p scattering, and neutrino-induced reactions [11–13]. In $\Lambda_c^+ \rightarrow \eta\pi^+\Lambda$ decays, discrepancies observed in the Dalitz plot may also originate from this state [14], and its inclusion significantly improves the fit to Belle data [15]. Similarly, in $\Lambda_c^+ \rightarrow p\bar{K}^0\eta$, the near-threshold enhancement in the $p\bar{K}^0$ mass spectrum is well reproduced by incorporating this low-lying $\Sigma(1/2^-)$ state, leading to better agreement with Belle measurements [16, 17]. Altogether, these findings provide strong evidence for the existence of a $\Sigma(1/2^-)$ resonance near 1380 MeV.

In addition to the $\Sigma(1/2^-)$ resonance around 1380 MeV, another $\Sigma(1/2^-)$ state located closer to the $\bar{K}N$ threshold has been proposed in various theoretical frameworks. The $\Lambda(1405)$ is widely interpreted as a $\bar{K}N$ bound state with dominant isoscalar components [4, 5, 18–21], and the potential existence of its isovector partner has also attracted considerable attention. For instance, the chiral unitary approach in Ref. [5] revealed two poles at 1401–40i MeV and 1488–114i MeV. More recent analyses based on covariant baryon chiral perturbation theory up to next-to-next-to-leading order [22] reinforced this two-pole picture, identifying a narrow pole at 1432–18i MeV, manifesting as a cusp-like structure near the $\bar{K}N$ threshold, along with a broader pole at 1364–110i MeV. Similarly, the coupled-channel calculations in Ref. [23]

*Electronic address: junhe@njnu.edu.cn

predicted both a narrow, higher-mass $\Sigma(1/2^-)$ state and a broader, lower-mass partner. These theoretical predictions receive additional support from the CLAS data on the $\gamma p \rightarrow K\Sigma\pi$ reaction [24, 25]. Moreover, Ref. [26] studied the decay $\Lambda_c^+ \rightarrow \pi^+\pi^0\pi^-\Sigma^+$ via a triangle loop mechanism, suggesting that a narrow $\Sigma(1/2^-)$ resonance with mass around 1430 MeV could manifest as a distinct peak near the $\bar{K}N$ threshold.

Recently, the Belle Collaboration reported a prominent structure around 1435 MeV, located near the $\bar{K}N$ threshold, in the $\Lambda\pi^+$ and $\Lambda\pi^-$ invariant mass spectra from the decay $\Lambda_c^+ \rightarrow \Lambda\pi^+\pi^+\pi^-$ [27]. In the present study, this structure is referred to as $\Sigma(1435)$. According to Belle's analysis, the data can be described using Breit-Wigner parametrizations, yielding a mass and width of 1434.3 ± 0.6 (stat) ± 0.9 (syst) MeV and 11.5 ± 2.8 (stat) ± 5.3 (syst) MeV in the $\Lambda\pi^+$ channel, and 1438.5 ± 0.9 (stat) ± 2.5 (syst) MeV with a broader width of 33.0 ± 7.5 (stat) ± 23.6 (syst) MeV in the $\Lambda\pi^-$ channel. Since both structures lie very close to the $\bar{K}N$ threshold, the possibility that they originate from a cusp effect was also considered. However, due to the limited statistical precision, the experimental analysis could not definitively discriminate between a genuine resonance and a threshold cusp. Nevertheless, the observed structure appears to be related to the longstanding features near the $\bar{K}N$ threshold that have been noted and discussed in the literature.

In the experimental analyses, the spin-parity of the observed structures was not considered. Nevertheless, the positions of these structures and their decays into $\Lambda\pi^\pm$ suggest they are consistent with a $\Sigma(1/2^-)$ assignment, as widely discussed in the literature. Notably, the experimental focus was mainly on the region near the $\bar{K}N$ threshold, and data below 1380 MeV were not included in the fit. Even the parameters of the well-established $\Sigma(1385)$ resonance were not treated with full rigor. In fact, a possible $\Sigma(1/2^-)$ resonance near 1380 MeV could interfere with the $\Sigma(1385)$, significantly complicating the interpretation and description of the complete $\Lambda\pi$ invariant mass spectrum.

Motivated by these considerations, the present study investigates the roles of both the $\Sigma(1380)$ and $\Sigma(1435)$ states with spin-parity $1/2^-$ in describing the Belle data on the $\Lambda\pi^\pm$ invariant mass spectra. As in the experimental analyses, the structure $\Sigma(1435)$ near the $\bar{K}N$ threshold is modeled using both a Breit-Wigner resonance and a rescattering cusp. However, in contrast to the experimental treatment, the spin-parity of $1/2^-$ is explicitly imposed for the $\Sigma(1435)$. The Breit-Wigner resonance contributions are described using effective Lagrangian methods, while the rescattering effects are incorporated through coupled-channel interactions: $\bar{K}^0 p$, $\pi^0\Sigma^+$, $\pi^+\Sigma^0$, $\pi^+\Lambda$, and $\eta\Sigma^+$ for the positively charged mode, and $K^- n$, $\pi^0\Sigma^-$, $\pi^-\Sigma^0$, $\pi^-\Lambda$, and $\eta\Sigma^-$ for the negatively charged mode. These interactions are treated within the framework of the quasipotential Bethe-Salpeter equation (qBSE) approach. Furthermore, unlike the experimental analyses that fitted the $\Lambda\pi^+$ and $\Lambda\pi^-$ spectra separately and neglected interference effects, the present work performs a simultaneous fit to both spectra and explicitly includes the interference among different contributions.

The remainder of this paper is organized as follows. Sec-

tion II presents the theoretical framework, including the decay mechanisms considered for $\Lambda_c \rightarrow \Lambda\pi^+\pi^+\pi^-$, the event simulation procedure, the effective Lagrangians used to describe Breit-Wigner resonances, the formulation of the interaction potential kernel, and a brief overview of the qBSE approach employed to account for rescattering effects. Section III provides the numerical results obtained from various fitting strategies. The roles of the $\Sigma(1435)$, treated either as a Breit-Wigner resonance or as a dynamically generated state via rescattering, along with the contribution of the additional $\Sigma(1380)$ resonance, are analyzed in detail. Finally, the main findings and their implications are summarized in Section IV.

II. THEORETICAL FRAME

In this section, the mechanism for the decay process $\Lambda_c^+ \rightarrow \Lambda\pi^+\pi^+\pi^-$ is first introduced. In the present analysis, the $\Sigma(1385)$ and $\Sigma(1380)$ are modeled as Breit-Wigner resonances with spin-parities $3/2^+$ and $1/2^-$, respectively, using effective Lagrangian formulations. In addition to the Breit-Wigner treatment, the $\Sigma(1435)$ structure is considered as a dynamically generated state arising from coupled-channel interactions, studied within the framework of the qBSE approach.

A. Decay mechanism of $\Lambda_c^+ \rightarrow \Lambda\pi^+\pi^+\pi^-$

The Belle data exhibit a prominent peak structure around 1380 MeV and a smaller enhancement near 1435 MeV. To describe these structures, two types of decay mechanisms are considered in the present work, as illustrated in Fig. 1.

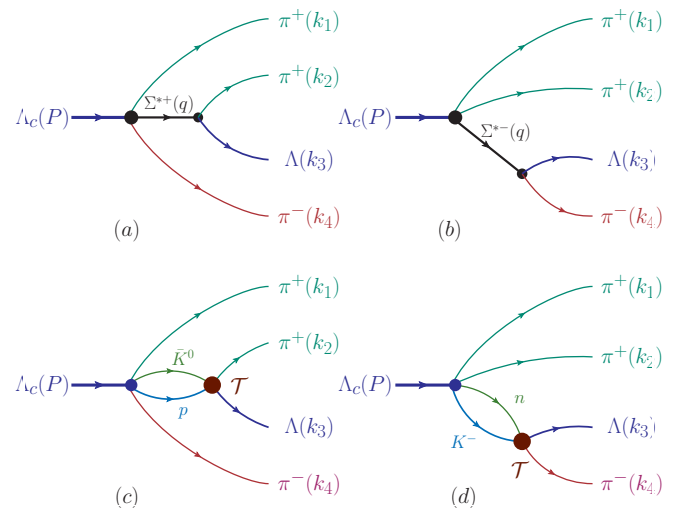


FIG. 1: Feynman diagrams for the decay $\Lambda_c^+ \rightarrow \Lambda\pi^+\pi^+\pi^-$. Panels (a) and (b) illustrate mechanisms involving intermediate Breit-Wigner resonances contributing to the $\Lambda\pi^+$ and $\Lambda\pi^-$ final states, respectively. Panels (c) and (d) show the corresponding mechanisms involving coupled-channel interactions for the positive and negative charge $\Lambda\pi^\pm$ systems. The brown filled circles denote the coupled-channel amplitudes \mathcal{T} .

In Fig. 1 (a) and (b), the decay mechanisms involving intermediate Breit-Wigner resonances are illustrated. In this mechanism, the Λ_c^+ first decays into a Σ^* resonance accompanied by two pions, and then the intermediate Σ^* subsequently decays into a Λ baryon and a pion. The intermediate resonance can carry either positive or negative charge, decaying into $\Lambda\pi^+$ and $\Lambda\pi^-$ final states, as shown in Fig. 1 (a) and (b), respectively.

In the present work, the Breit-Wigner formalism is used to describe the $\Sigma(1380)$, $\Sigma(1385)$, and $\Sigma(1435)$. However, an alternative approach is also adopted, where the $\Sigma(1435)$ is treated as a dynamically generated structure arising from coupled-channel interactions, as illustrated in Fig. 1 (c) and (d). In this mechanism, the Λ_c^+ first decays into two pions and a $\bar{K}N$ pair. Since the primary focus is on the $\Sigma(1435)$ structure, only the $\bar{K}N$ channel is considered in the initial Λ_c^+ decay. Similar to the Breit-Wigner case, rescattering effects can occur in both the positive and negative charge channels. In the positive charge channel, the $\bar{K}^0 p$ system connects to the final $\Lambda\pi^+$ state through a coupled-channel rescattering process, involving channels $\bar{K}^0 p$, $\pi^0\Sigma^+$, $\pi^+\Sigma^0$, $\pi^+\Lambda$, and $\eta\Sigma^+$. The negative charge channel proceeds analogously.

The total amplitude for the decay can be expressed as

$$\mathcal{M} = \sum_{\Sigma^{*\pm}} \left(e^{i2\pi\phi_{\Sigma^{*+}}} \mathcal{M}_{\Sigma^{*+}} + e^{i2\pi\phi_{\Sigma^{*-}}} \mathcal{M}_{\Sigma^{*-}} \right) + \mathcal{M}_{\text{bk}}, \quad (1)$$

where $e^{i2\pi\phi_{\Sigma^{*\pm}}}$ and $\mathcal{M}_{\Sigma^{*\pm}}$ denote the relative phases and amplitudes associated with the charge positive and negative resonance $\Sigma^{*\pm}$, respectively. This notation can also be used when describing contributions from rescattering mechanisms.

In the present analysis, following the experimental procedure, the two identical π^+ mesons are treated as indistinguishable. Consequently, the amplitudes involving the positive charge channel must be symmetrized as

$$\mathcal{M}_{\Sigma^{*+}} = \frac{1}{\sqrt{2}} [\mathcal{M}_{\Sigma^{*+}}(1234) + (2 \leftrightarrow 1)], \quad (2)$$

where $\mathcal{M}_{\Sigma^{*+}}(1234)$ represents the amplitude corresponding to the diagrams shown in Fig. 1(a) or 1(c), with the indices (1234) labeling the final particles. For the negative charge channel, the two π^+ mesons have already been symmetrized in the definition of the amplitude, and thus no additional treatment is required.

All other contributions are treated as a constant background term, given by

$$i\mathcal{M}_{\text{bk}} = g_{\text{bk}} \bar{u}_{\Lambda} u_{\Lambda_c}, \quad (3)$$

where g_{bk} is a free parameter and u_{Λ_c} and u_{Λ} are the Dirac spinors for the Λ_c^+ and Λ baryons, respectively. Additionally, to account for possible trends in the higher invariant mass region of the $\Lambda\pi^{\pm}$ spectra, a first-order Chebyshev polynomial modification of the background is also considered in the current work, written as $1 + cM$, where M is the invariant mass of the $\Lambda\pi^{\pm}$ system. Considering that the phase space factor is included explicitly in the current treatment, a first-order polynomial is adopted instead of a second-order one, which is different from that adopted in the Belle analyses [27].

With the decay amplitude, the differential decay width can be written as

$$d\Gamma = \frac{1}{2E} \sum |\mathcal{M}|^2 d\Phi, \quad (4)$$

where E is the energy of the initial Λ_c^+ baryon, and $d\Phi$ represent the Lorentz-invariant phase space elements. In this work, the phase space element $d\Phi$ is simulated using the method proposed in Ref. [28], implemented in the Julia programming language. The corresponding Julia package is available on GitHub [29]. A total of 10^8 events were generated for the simulation. The momenta of the final-state particles are sampled using a Monte Carlo approach that strictly enforces energy-momentum conservation. From these simulated momenta, the invariant mass spectra of the $\Lambda\pi^{\pm}$ systems are constructed and subsequently used in the analysis.

B. Amplitudes with intermediate Breit-Wigner resonances

The amplitudes for the diagrams involving Breit-Wigner resonances [see Fig. 1 (a) and (b)] are derived using standard Feynman rules based on effective Lagrangians. In this work, the $\Sigma(1385)$ and $\Sigma(1380)$ are all treated as Breit-Wigner resonances, and this is also one of the two scenarios considered for the $\Sigma(1435)$. Among these, the $\Sigma(1385)$ is assigned a spin-parity of $3/2^+$, while both the $\Sigma(1380)$ and $\Sigma(1435)$ are considered to have spin-parity $1/2^-$.

For the intermediate Σ^* resonance with $J^P = 3/2^+$, the effective Lagrangians describing the Λ_c decay into $\Sigma(3/2^+)$ plus two pions, and the subsequent $\Sigma(3/2^+)$ decay into $\Lambda\pi$ are written as [30, 31]

$$\begin{aligned} \mathcal{L}_{\Lambda_c \Sigma(3/2^+) \pi\pi} &= \frac{i}{m_{\pi}} \bar{\Sigma}_{\mu} (\pi \partial^{\mu} \pi' + \pi' \partial^{\mu} \pi) (g_{\Sigma(3/2^+)}^{PV} - g_{\Sigma(3/2^+)}^{PC} \gamma_5) \Lambda_c, \\ \mathcal{L}_{\Sigma(3/2^+) \Lambda\pi} &= -\frac{i g_{\Sigma(3/2^+)}}{m_{\pi}} \bar{\Lambda} \partial^{\mu} \pi \Sigma_{\mu}, \end{aligned} \quad (5)$$

where π and π' denote the two pions, and $g_{\Sigma(3/2^+)}^{PV}$ and $g_{\Sigma(3/2^+)}^{PC}$ are the coupling constants for parity-violating and parity-conserving interactions, respectively. Since it is a weak decay, these couplings may differ for $\Sigma(3/2^+)$ states of different charges.

The propagator for a spin-3/2 particle is taken as

$$\begin{aligned} G_{\mu\nu}(q) &= \frac{i}{q^2 - m^2 + im\Gamma} (\not{q} + m) [-g_{\mu\nu} \\ &+ \frac{1}{3} \gamma_{\mu} \gamma_{\nu} + \frac{1}{3m} (\gamma_{\mu} q_{\nu} - \gamma_{\nu} q_{\mu}) + \frac{2}{3m^2} q_{\mu} q_{\nu}], \end{aligned} \quad (6)$$

where q and m are the four-momentum and mass of the spin-3/2 particle, and Γ is its decay width.

Following the Feynman rules, the corresponding amplitude can be obtained as

$$i\mathcal{M}_{\Sigma(3/2^{\pm})} = g_{\Sigma^*(3/2^{\pm})} \frac{\bar{\Lambda} \Delta_3^{\pm} (1 - \gamma_5) \Lambda_c}{q^2 - m_{\Sigma(3/2^{\pm})}^2 + im_{\Sigma(3/2^{\pm})} \Gamma_{\Sigma(3/2^{\pm})}}, \quad (7)$$

with

$$\Delta_3^\pm = (\not{k} + m_{\Sigma(3/2^+)^\pm})[-k \cdot p + \frac{1}{3}k\not{p} + \frac{1}{3m_{\Sigma(3/2^+)^\pm}}(kq \cdot p - \not{p}q \cdot k) + \frac{2}{3m_{\Sigma(3/2^+)^\pm}^2}q \cdot kq \cdot p], \quad (8)$$

where $p = k_1 + k_4$ or $k_1 + k_2$ corresponds to the cases of charge positive and negative $\Sigma(3/2^+)$, respectively. Following the literature, the coupling constants are set equal, i.e., $g_{\Sigma(3/2^+)^\pm}^{PV} = g_{\Sigma(3/2^+)^\pm}^{PC}$, for simplicity [30–32]. This treatment simplifies the fitting process by reducing the number of free parameters while effectively capturing the strength of the $\Sigma(3/2^+)$ contributions. In the fitting procedure, the coupling constants are absorbed into an effective parameter, defined as

$$g_{\Sigma(3/2^+)^\pm} = -\frac{g_{\Sigma(3/2^+)^\pm}^{PC}g_{\Sigma(3/2^+)^\pm}^{PC}}{m_\pi^2}. \quad (9)$$

If the intermediate Σ^* states have spin-parity $1/2^-$, the effective Lagrangians describing the Λ_c decay and the subsequent $\Sigma(1/2^-)$ decay can be written as [30]

$$\begin{aligned} \mathcal{L}_{\Lambda_c \Sigma(1/2^-) \pi \pi} &= i\bar{\Sigma}\pi\pi(g_{\Sigma(1/2^-)}^{PV} - g_{\Sigma(1/2^-)}^{PC}\gamma_5)\Lambda_c, \\ \mathcal{L}_{\Sigma(1/2^-) \Lambda \pi} &= -ig_{\Sigma(1/2^-)}\bar{\Lambda}\pi\Sigma, \end{aligned} \quad (10)$$

where $g_{\Sigma(1/2^-)}^{PV}$ and $g_{\Sigma(1/2^-)}^{PC}$ are the coupling constants associated with parity-violating and parity-conserving interactions, respectively, and are also taken to be equal.

Following the standard Feynman rules, the decay amplitude can be obtained as

$$i\mathcal{M}_{\Sigma(1/2^-)^\pm} = g_{\Sigma(1/2^-)^\pm} \frac{\bar{\Lambda}\Delta^\pm(1 - \gamma_5)\Lambda_c}{q^2 - m_{\Sigma(1/2^-)^\pm}^2 + im_{\Sigma(1/2^-)^\pm}\Gamma_{\Sigma(1/2^-)^\pm}}, \quad (11)$$

where Δ is given by $\Delta^\pm = (\not{k} + m_{\Sigma(1/2^-)^\pm})$. In the fitting procedure, the combination of coupling constants is also treated as a single effective parameter, defined as $g_{\Sigma(1/2^-)^\pm} = g_{\Sigma(1/2^-)^\pm}^{PC}g_{\Sigma(1/2^-)^\pm}^{PC}$.

C. Amplitudes with rescattering

For the structure observed around 1435 MeV, two scenarios, a Breit-Wigner resonance and a coupled-channel rescattering process, are considered in the current work. In the rescattering mechanism, the coupled-channel interactions among the channels $\bar{K}^0 p$, $\pi^0 \Sigma^+$, $\pi^+ \Sigma^0$, $\pi^+ \Lambda$, and $\eta \Sigma^+$ for the positively charged mode, and $K^- n$, $\pi^0 \Sigma^-$, $\pi^- \Sigma^0$, $\pi^- \Lambda$, and $\eta \Sigma^-$ for the negatively charged mode, are taken into account. These interactions correspond to the isovector counterpart of the dynamics associated with the $\Lambda(1405)$ resonance, and have been established in Ref. [18]. The interaction kernel between different channels is given by

$$i\mathcal{V}_{\lambda\lambda'}^{kl} = -C^{kl} \frac{1}{4f^2} \bar{u}_{\lambda'}(p)\gamma^\mu u_\lambda(p')(k_\mu + k'_\mu), \quad (12)$$

where $u_{\lambda'}(p')$ and $\bar{u}_\lambda(p)$ are the Dirac spinors for the incoming and outgoing baryons, respectively, while $k^{(\prime)}$ and $p^{(\prime)}$ denote the momenta of the mesons and baryons involved in the initial and final states.

The coefficients C^{kl} represent the channel-dependent coupling strengths determined by chiral symmetry constraints, with their explicit values given in Ref. [18]. In that work, the potential was derived within a chiral unitary approach and applied through a coupled-channel Lippmann–Schwinger equation, using $f = 1.15f_\pi$ with $f_\pi = 93$ MeV. In the present study, a different framework is adopted based on the qBSE. The same chiral potential has been used in the qBSE framework to investigate the $\Lambda(1405)$ resonance and to describe low-energy cross sections for the processes $K^- p \rightarrow K^- p$, $\bar{K}^0 n$, $\pi^0 \Lambda$, $\pi^0 \Sigma^0$, $\pi^+ \Sigma^-$, and $\pi^- \Sigma^+$, yielding a good agreement with experimental data [33]. For consistency, this value is also adopted in the current analysis.

The rescattering amplitude \mathcal{T} , as illustrated in Fig. 1(c) and (d), can be obtained by inserting the potential kernel into the Bethe-Salpeter equation. By employing the quasipotential approximation and performing a partial wave decomposition, the original four-dimensional integral equation in Minkowski space can be reduced to a one-dimensional integral equation for each spin-parity J^P channel [34–38], as follows,

$$\begin{aligned} i\mathcal{T}_{\lambda\lambda'}^{J^P}(\mathbf{p}', \mathbf{p}) &= i\mathcal{V}_{\lambda\lambda'}^{J^P}(\mathbf{p}', \mathbf{p}) + \frac{1}{2} \sum_{\lambda''} \int \frac{p''^0 d\mathbf{p}''}{(2\pi)^3} \\ &\cdot i\mathcal{V}_{\lambda'\lambda''}^{J^P}(\mathbf{p}', \mathbf{p}'')G_0(p'')i\mathcal{M}_{\lambda''\lambda}^{J^P}(\mathbf{p}'', \mathbf{p}), \end{aligned} \quad (13)$$

where λ , λ' , and λ'' denote the helicities of the initial, final, and intermediate baryons, respectively. The helicities of the pseudoscalar mesons are omitted.

The propagator $G_0(p'')$ is reduced from its original four-dimensional form by the quasipotential approximation. It is given by

$$\begin{aligned} G_0 &= \frac{\delta^+(p_h''^2 - m_h^2)}{p_l''^2 - m_l^2} \\ &= \frac{\delta^+(p_h''^0 - E_h(p''))}{2E_h(p'')[(W - E_h(p''))^2 - E_l^2(p'')]}, \end{aligned} \quad (14)$$

where p_h'' and p_l'' are the four-momenta of the heavier and lighter particles in the intermediate state, respectively, and W denotes the total center-of-mass energy. In this work, the spectator approximation is adopted, where the heavier particle (denoted as h) is placed on-shell [39], satisfying $p_h''^0 = E_h(p'') = \sqrt{m_h^2 + \mathbf{p}''^2}$. Consequently, the energy of the lighter particle l is determined by $p_l''^0 = W - E_h(p'')$. Here and throughout this paper, the three-momentum magnitude in the center-of-mass frame is denoted as $p = |\mathbf{p}|$.

The partial-wave potential $\mathcal{V}_{\lambda\lambda'}^{J^P}(\mathbf{p}', \mathbf{p})$ is obtained from the interaction potential $\mathcal{V}_{\lambda\lambda'}(\mathbf{p}', \mathbf{p})$ through the partial wave projection as

$$\mathcal{V}_{\lambda\lambda'}^{J^P}(\mathbf{p}', \mathbf{p}) = 2\pi \int d\cos\theta [d_{\lambda\lambda'}^J(\theta)\mathcal{V}_{\lambda\lambda'}(\mathbf{p}', \mathbf{p})]$$

$$+ \eta d_{-\lambda\lambda'}^J(\theta) \mathcal{V}_{\lambda-\lambda}(\mathbf{p}', \mathbf{p})], \quad (15)$$

where $d_{\lambda\lambda'}^J(\theta)$ are the Wigner d functions describing the rotation between initial and final helicity states, and θ is the scattering angle between the initial and final three-momenta. The factor η is given by $\eta = PP_1P_2(-1)^{J-J_1-J_2}$ where P is the intrinsic parity of the system, P_1 and P_2 are the parities of the two constituent particles, and J, J_1, J_2 are the total and individual spins, respectively. The initial and final three-momenta are chosen as $\mathbf{p} = (0, 0, p)$ and $\mathbf{p}' = (p' \sin \theta, 0, p' \cos \theta)$ for convenience in performing the partial wave expansion. In addition, an exponential form factor is introduced into the propagator to regularize the high-momentum behavior $G_0(\mathbf{p}'') \rightarrow G_0(\mathbf{p}'') e^{-2(p''^2 - m^2)^2 / \Lambda_r^4}$ where Λ_r is the cutoff parameter controlling the regularization strength [35].

The total decay amplitude corresponding to Fig. 1(c) is obtained by incorporating the rescattering amplitude \mathcal{T} into the decay process as follows:

$$i\mathcal{M}_{\lambda\lambda\Lambda_c}(k_2, k_3) = \sum_{\lambda'} \int \frac{d^3k_3'}{(2\pi)^3} i\mathcal{T}_{\lambda\lambda'}(k_2, k_3; k_2', k_3') \cdot G_0(k_3) i\mathcal{A}_{\lambda\lambda\Lambda_c}(k_2', k_3'), \quad (16)$$

where $\lambda_{\Lambda_c}, \lambda$, and λ' denote the helicities of the initial Λ_c , the final-state Λ , and the intermediate nucleon, respectively. The helicities of the pseudoscalar mesons are neglected, as they are not relevant for the current analysis. The momenta $k_2^{(\prime)}$ and $k_3^{(\prime)}$ correspond to the final (or intermediate) π^+ and Λ , respectively. For the diagram in Fig. 1(d), π^+ should be replaced by π^- , labeled with momentum k_4 . Other momenta not directly involved in the rescattering process are omitted for brevity.

However, since the rescattering amplitude is obtained in a partial-wave-decomposed form, a partial wave decomposition of the decay amplitude is also performed. This leads to the expression:

$$i\mathcal{M}_{\lambda\lambda\Lambda_c}(k_2, k_3) = \sum_J N_J \sum_{\lambda'} \int \frac{k_3'^2 dk_3'}{(2\pi)^3} i\mathcal{T}_{\lambda\lambda'}^J(k_3', M_{23}) \cdot G_0(k_3) i\mathcal{A}_{\lambda\lambda\Lambda_c}^{J\lambda}(k_3', M_{23}), \quad (17)$$

where $N_J = \sqrt{(2J+1)/(4\pi)}$, and $M_{23} = \sqrt{(k_2 + k_3)^2}$ is the invariant mass of the $\pi^+\Lambda$ system.

After including the parity quantum number, the decay amplitude can be rewritten as:

$$i\mathcal{M}_{\lambda\lambda\Lambda_c}(k_2, k_3) = \sum_{J^P} \frac{N_J^2}{4} \int \frac{k_3'^3 dk_3'}{(2\pi)^3} \sum_{\lambda'} \cdot i\mathcal{T}_{\lambda\lambda'}^{J^P}(k_3', M_{23}) G_0(k_3) i\mathcal{A}_{\lambda\lambda\Lambda_c}^{J^P\lambda}(k_3', M_{23}). \quad (18)$$

The Lagrangian describing the initial weak decay process $\Lambda_c \rightarrow \pi\pi\bar{K}N$ is given by

$$\mathcal{L}_{\Lambda_c N \pi \pi \bar{K}} = i\bar{N}\pi\pi\bar{K}(g^{PV} - g^{PC}\gamma_5)\Lambda_c, \quad (19)$$

where g^{PV} and g^{PC} denote the parity-violating and parity-conserving coupling constants, respectively. They are also

taken to be equal to a common value g^P , which is further denoted as $g_{\Sigma(1435)^\pm}$ for consistency with the Breit-Wigner scenario.

To match the partial-wave representation used in the rescattering amplitude, the helicity amplitude for the initial Λ_c decay is also decomposed into partial waves. The corresponding expression is

$$\mathcal{A}_{\lambda'\lambda\Lambda_c}^{P\lambda} = \int d\Omega_J [D_{\lambda\lambda'}^J(\Omega), \mathcal{A}_{\lambda'\lambda\Lambda_c} + \eta D_{\lambda-\lambda'}^J(\Omega) \mathcal{A}_{-\lambda'\lambda\Lambda_c}], \quad (20)$$

where $\lambda_{\Lambda_c}, \lambda'$, and λ are the helicities of the initial Λ_c , the intermediate nucleon, and the $\pi\Lambda$ system, respectively. The Wigner D -functions $D_{\lambda\lambda'}^J(\Omega)$ project the helicity amplitude $\mathcal{A}_{\lambda'\lambda\Lambda_c}$ into states of definite total angular momentum J and parity P , and η is the intrinsic parity factor as defined above.

III. NUMERICAL RESULTS

A. Fitting procedure

This section presents a detailed fitting analysis of the Belle data to investigate the possible role of the $\Sigma(1/2^-)$ resonances in the decay process $\Lambda_c \rightarrow \Lambda\pi^-\pi^+\pi^+$. The fitting results are summarized in Table I. The $\Lambda\pi^+$ invariant mass spectrum exhibits a prominent peak around 1380 MeV, which may receive contributions from both the $\Sigma(1385)$ resonance with spin-parity $J^P = 3/2^+$ and the hypothesized $\Sigma(1380)$ resonance with $J^P = 1/2^-$. The $\Sigma(1385)$ is a well-established state with a three-star rating from the PDG and is therefore included by default in all fitting scenarios to ensure a consistent description of the dominant feature in the spectrum.

In contrast, the $\Sigma(1380)$ is less well established and is typically considered a broad resonance in the literature. Due to its large width, its contribution tends to be smeared out in the spectrum, resulting in relatively low sensitivity to its exact mass and width during the fitting procedure. To avoid introducing unnecessary free parameters, its mass and width are fixed to 1380 and 120 MeV, respectively, following the values adopted in previous studies [7, 9, 15, 40].

Given the dominant contribution of the $\Sigma(1385)$ resonance to the spectrum, the analysis begins with a baseline fit, labeled (00) in Table I, which includes only the $\Sigma(1385)$ and a nonresonant background component. To further investigate the origin of the structure observed around 1435 MeV, the $\Sigma(1435)$ resonance is introduced into the fitting framework. Since the Belle Collaboration applied a selection cut to enhance the signal in their analysis, two corresponding fits are performed: one using the partial data points between 1.38 and 1.53 GeV, denoted as $(01_{\text{BW}})^P$, and another using the full data set, denoted as (01_{BW}) . In both cases, the $\Sigma(1435)$ is treated as a Breit-Wigner resonance.

To explore the possibility that the $\Sigma(1435)$ is not a conventional Breit-Wigner resonance but rather a dynamically generated state arising from coupled-channel interactions, an additional fit is performed in which the $\Sigma(1435)$ contribution

TABLE I: Fitting parameters and χ^2 values for different scenarios labeled as (ij) , where i and j indicate the inclusion (1) or exclusion (0) of the $\Sigma(1380)$ and $\Sigma(1435)$ resonances, respectively. The subscript “BW” refers to cases where the $\Sigma(1435)$ is treated as a Breit-Wigner resonance, while “RS” denotes a rescattering model. The superscript “p” indicates fits performed using a subset of the data. The strength parameters g for the resonances, rescattering contribution, and background (bk) are scaled to match the overall event yield; therefore, their absolute values have no physical units and only their relative magnitudes are meaningful. The phase parameters ϕ are dimensionless. The background shape parameters c_{\pm} are given in units of GeV^{-1} , and the masses m and widths Γ are in units of MeV. The χ^2_{-} and χ^2_{+} values correspond to the fits for the $\Lambda\pi^{-}$ and $\Lambda\pi^{+}$ invariant mass spectra, respectively. The total fit quality is indicated by χ^2_{tot} , along with the total number of data points and the number of degrees of freedom (ndf).

Fits	(00)	(01 _{BW}) ^p	(01 _{BW})	(01 _{RS})	(11 _{BW})	(11 _{RS})	(10)	Reference
$g_{\Sigma(1380)^{-}}$	--	--	--	--	0.0000	0.0149	0.0000	
$\phi_{\Sigma(1380)^{-}}$	--	--	--	--	0.0231	0.5611	0.0297	
$g_{\Sigma(1380)^{+}}$	--	--	--	--	0.0151	0.0107	0.0161	
$\phi_{\Sigma(1380)^{+}}$	--	--	--	--	0.2706	0.4282	0.2656	
$g_{\Sigma(1385)^{-}}$	0.3016	0.2666	0.2984	0.3259	0.2976	0.3356	0.2993	
$\phi_{\Sigma(1385)^{-}}$	0.7290	0.7211	0.7301	0.7765	0.7276	0.7229	0.7187	
$m_{\Sigma(1385)^{-}}$	1384.8	1386.6	1386.1	1384.3	1384.7	1385.3	1384.7	1387.2 ± 0.5 [1]
$\Gamma_{\Sigma(1385)^{-}}$	34.6	30.8	34.5	36.5	33.0	37.1	33.8	39.4 ± 2.1 [1]
$g_{\Sigma(1385)^{+}}$	0.4824	0.4662	0.4640	0.4146	0.3224	0.3645	0.3313	
$\phi_{\Sigma(1385)^{+}}$	0.2677	0.2727	0.2738	0.4052	0.2763	0.2741	0.2779	
$m_{\Sigma(1385)^{+}}$	1378.6	1378.4	1378.8	1380.4	1380.5	1381.1	1380.7	1382.83 ± 0.34 [1]
$\Gamma_{\Sigma(1385)^{+}}$	41.0	39.3	40.0	36.8	30.1	34.0	31.4	36.2 ± 0.7 [1]
$g_{\Sigma(1435)^{-}}$	--	0.00043	0.00037	8.5904	0.00037	9.6326	--	
$\phi_{\Sigma(1435)^{-}}$	--	0.1883	0.1253	0.7513	0.1539	0.8291	--	
$m_{\Sigma(1435)^{-}}$	--	1434.7	1433.5	--	1433.5	--	--	1438.5 ± 0.9 [27]
$\Gamma_{\Sigma(1435)^{-}}$	--	11.9	11.5	--	11.5	--	--	33.0 ± 7.5 [27]
$g_{\Sigma(1435)^{+}}$	--	0.00093	0.00097	7.515	0.00066	7.2618	--	
$\phi_{\Sigma(1435)^{+}}$	--	0.2755	0.3354	0.7577	0.3510	0.8252	--	
$m_{\Sigma(1435)^{+}}$	--	1435.1	1438.0	--	1438.0	--	--	1434.3 ± 0.6 [27]
$\Gamma_{\Sigma(1435)^{+}}$	--	14.2	18.5	--	12.6	--	--	11.5 ± 2.8 [27]
g_{bk}	1.3012	1.3010	1.3009	1.1860	1.2894	1.1896	1.2894	
c_{-}	0.0217	0.0206	0.0224	0.0045	-0.0135	0.0243	-0.0104	
c_{+}	-0.0870	-0.0867	-0.0880	-0.0872	-0.1081	-0.0900	-0.1080	
$\chi^2_{-}/N_{\Lambda\pi^{-}}$	276/100	97/75	156/100	216/100	156/100	137/100	215/100	
$\chi^2_{+}/N_{\Lambda\pi^{+}}$	556/100	106/75	262/100	235/100	153/100	154/100	294/100	
$\chi^2_{\text{tot}}/N_{\text{tot}}$	832/200	203/150	418/200	451/200	309/200	291/200	509/200	
$\chi^2_{\text{tot}}/\text{ndf}$	4.40	1.55	2.31	2.43	1.75	1.61	2.81	

is modeled via a rescattering mechanism. This fit is referred to as (01_{RS}).

The impact of the $\Sigma(1380)$ resonance is further examined by including both the $\Sigma(1385)$ and $\Sigma(1380)$ in the model. When the $\Sigma(1435)$ is incorporated as a Breit-Wigner resonance, the corresponding fit is labeled as (11_{BW}); when it is instead treated through rescattering, the fit is denoted as (11_{RS}). To isolate the role of the $\Sigma(1380)$, another fit is carried out that includes the $\Sigma(1385)$ and $\Sigma(1380)$, but excludes the $\Sigma(1435)$ entirely; this scenario is labeled (10).

The fitted parameters are summarized in Table I. For the $\Sigma(1380)$ resonance, the mass and width are fixed during the fit, and only the coupling strengths $g_{\Sigma(1380)\pm}$ and the relative phases $\phi_{\Sigma(1380)\pm}$ are treated as free parameters. In cases where the $\Sigma(1385)$ and $\Sigma(1435)$ are modeled as Breit-Wigner resonances, their masses m and widths Γ are also treated as fit parameters, in addition to their respective strengths and phases. To account for nonresonant background contributions, three additional parameters are introduced: the overall strength g_{bk} and the shape parameters c_- and c_+ . A common normalization factor is applied to all resonance and background strengths g to ensure consistency with the total event yield observed in the experimental data. Consequently, only the relative magnitudes of these parameters carry physical significance, while their absolute values are not meaningful. The quality of each fit is evaluated using the corresponding χ^2 values. Specifically, χ^2_- and χ^2_+ are reported for the $\Lambda\pi^-$ and $\Lambda\pi^+$ invariant mass distributions, respectively, each accompanied by the number of data points used. The total χ^2_{tot} , along with the total number of data points and the number of degrees of freedom, is also provided to quantify the overall fit quality.

B. Role of $\Sigma(1435)$

Figure 2 shows the fits to the $\Lambda\pi^\pm$ invariant mass spectra with and without the inclusion of the $\Sigma(1435)$ resonance. Three fitting schemes are considered: (00), (01_{BW})^P, and (01_{BW}). In fit (00), only the $\Sigma(1385)$ with spin-parity $J^P = 3/2^+$ and a non-resonant background are included. This minimal setup is sufficient to reproduce the overall structure observed in the Belle data for both the $\Lambda\pi^-$ and $\Lambda\pi^+$ channels.

The corresponding χ^2 values for each data point are also provided under fit (00). In the $\Lambda\pi^-$ spectrum, the majority of the data points exhibit small χ^2 values, indicating a good fit in general. However, significant discrepancies are observed in the vicinity of 1435 MeV, where the χ^2 values are notably larger. A few data points near the lower mass region around 1350 MeV also show elevated χ^2 . Similarly, in the $\Lambda\pi^+$ spectrum, large χ^2 values are concentrated around 1435 MeV and extend down to the 1350–1380 MeV range. Additional discrepancies are observed in the high-mass region near 1.55 GeV. The theoretical curves for invariant mass spectrum show clear deviations from the experimental data, particularly around 1345 MeV.

The clear deviation from experimental data around 1435 MeV suggests the presence of a resonance with a mass near 1435 MeV. In Fig. 2, the results of the fit (01)_{BW}, which

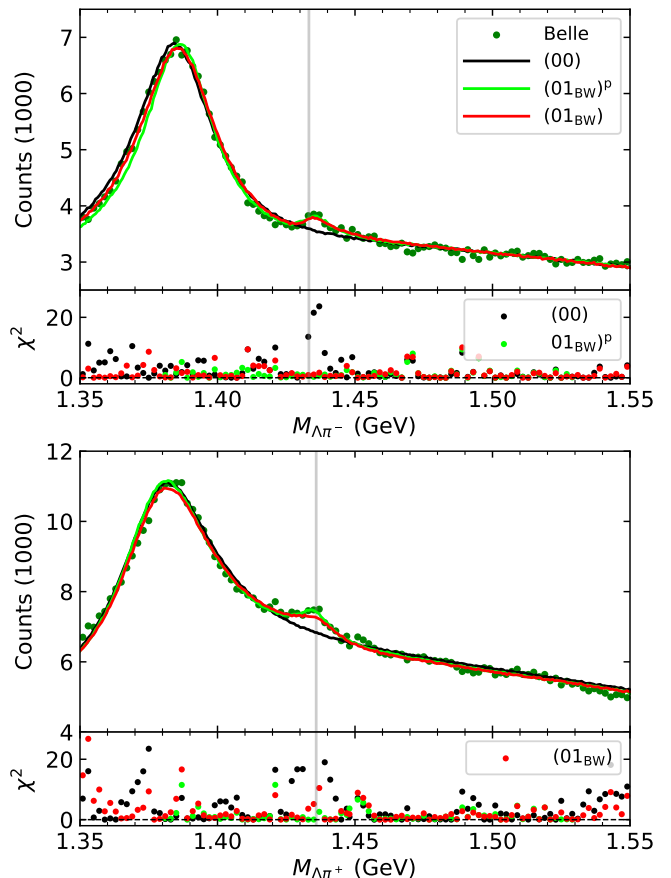


FIG. 2: Invariant mass spectra of $\Lambda\pi^-$ (upper panel) and $\Lambda\pi^+$ (lower panel). The curves correspond to the fit results for three scenarios: (00) including only the $\Sigma(1385)$ and background (black); (01_{BW})^P including the $\Sigma(1435)$ and using partial data (green); and (01_{BW}) including the $\Sigma(1435)$ with the full data set (red). The data are taken from the Belle Collaboration [27]. The vertical grey lines indicate the K^-n and \bar{K}^0p thresholds. The scatter points in the lower part of each panel represent the individual χ^2 contributions of the corresponding data points. Legends apply to both panels.

includes the $\Sigma(1435)$ modeled as a Breit-Wigner resonance, are presented. A substantial reduction in the χ^2 value is observed, indicating a significant improvement in the fit quality—particularly in the region near 1435 MeV—where the model now better reproduces the experimental event distribution. As summarized in Table I, the total χ^2 values for the $\Lambda\pi^-$ and $\Lambda\pi^+$ spectra in the baseline fit (00) are 276 and 556, respectively, leading to a combined $\chi^2_{\text{tot}}/\text{ndf}$ of 4.40. When the $\Sigma(1435)$ is included as a Breit-Wigner resonance, the total $\chi^2_{\text{tot}}/\text{ndf}$ decreases significantly to 2.31, with the individual contributions reduced to 156 for the $\Lambda\pi^-$ spectrum and 263 for the $\Lambda\pi^+$ spectrum. The relatively larger χ^2 value for the $\Lambda\pi^-$ channel mainly arises from discrepancies in the lower energy region, where the fit exhibits poorer agreement with the experimental data.

Results based on the partial dataset in the range 1.38–1.53 GeV are also presented, following the strategy adopted

in the Belle analysis, which specifically targets the $\Sigma(1435)$ region. In this case, the χ^2 values for the $\Lambda\pi^-$ and $\Lambda\pi^+$ spectra are 97 and 106, respectively, comparable to the Belle Collaboration's reported values of 74 and 93 [27]. The present analysis employs 19 fit parameters, a number similar to the 18 used in the Belle study. Furthermore, both the $\Lambda\pi^-$ and $\Lambda\pi^+$ spectra are fitted simultaneously, with interference effects among different contributions explicitly taken into account. As such, the current fitting procedure is comparable to the Belle analysis in terms of both complexity and reliability. Notably, even when the full dataset is used, the average χ^2 remains close to that obtained from the partial dataset, further demonstrating the robustness of the fit.

The masses and widths of both the $\Sigma(1385)$ and $\Sigma(1435)$ are fitted in the $(01_{\text{BW}})^{\text{P}}$ and (01_{BW}) scenarios. For the $\Sigma(1385)$, the fitted mass and width for the negatively charged state are 1386.6 MeV and 30.8 MeV in the $(01_{\text{BW}})^{\text{P}}$ fit, and 1386.1 MeV and 34.5 MeV in the (01_{BW}) fit. For the positively charged state, the corresponding values are 1378.4 MeV and 39.3 MeV in $(01_{\text{BW}})^{\text{P}}$, and 1378.8 MeV and 40.0 MeV in (01_{BW}) . These values are consistent with those reported by the PDG [1]. For the $\Sigma(1435)$, the fitted mass and width are 1434.7 and 11.9 MeV for the negatively charged state, and 1435.1 and 14.2 MeV for the positively charged state. Compared with the measurements reported by the Belle Collaboration [27], the widths of the two charge states in our fit show better consistency with each other.

C. Breit-Wigner vs rescattering for $\Sigma(1435)$ structure

The $\Sigma(1385)$ provides the dominant contribution in the energy region covered by the Belle experiment. Once the $\Sigma(1435)$ structure is included as a Breit-Wigner resonance, the experimental data are well reproduced. Two scenarios are considered for modeling the $\Sigma(1435)$: one treats it as a Breit-Wigner resonance, as implemented in the fit labeled (01_{BW}) , and the other describes it via a rescattering mechanism, corresponding to the fit (01_{RS}) . The results for the rescattering scenario are summarized in Table I. Compared with the baseline fit (00), which includes only the $\Sigma(1385)$ and background contributions, the rescattering scenario yields a substantial reduction in the total χ^2 , decreasing from 832 to 451 for the full dataset. Although this is slightly higher than the value obtained in the Breit-Wigner case, it still represents a significant improvement in fit quality. Notably, the fitted parameters for the $\Sigma(1385)$ remain nearly unchanged across the different scenarios. No explicit resonance parameters are associated with the $\Sigma(1435)$ in the rescattering fit, since its contribution arises dynamically rather than from a predefined Breit-Wigner form.

As shown in Fig. 3, the fitted invariant mass spectra from both scenarios are nearly indistinguishable and provide a good description of the experimental data, except in the low-energy region of the $\Lambda\pi^+$ spectrum, where some discrepancies persist. The individual contributions from the $\Sigma(1385)$, $\Sigma(1435)$, and background are also displayed in Fig. 3. Although the total fit results are similar for both mechanisms, the decomposition

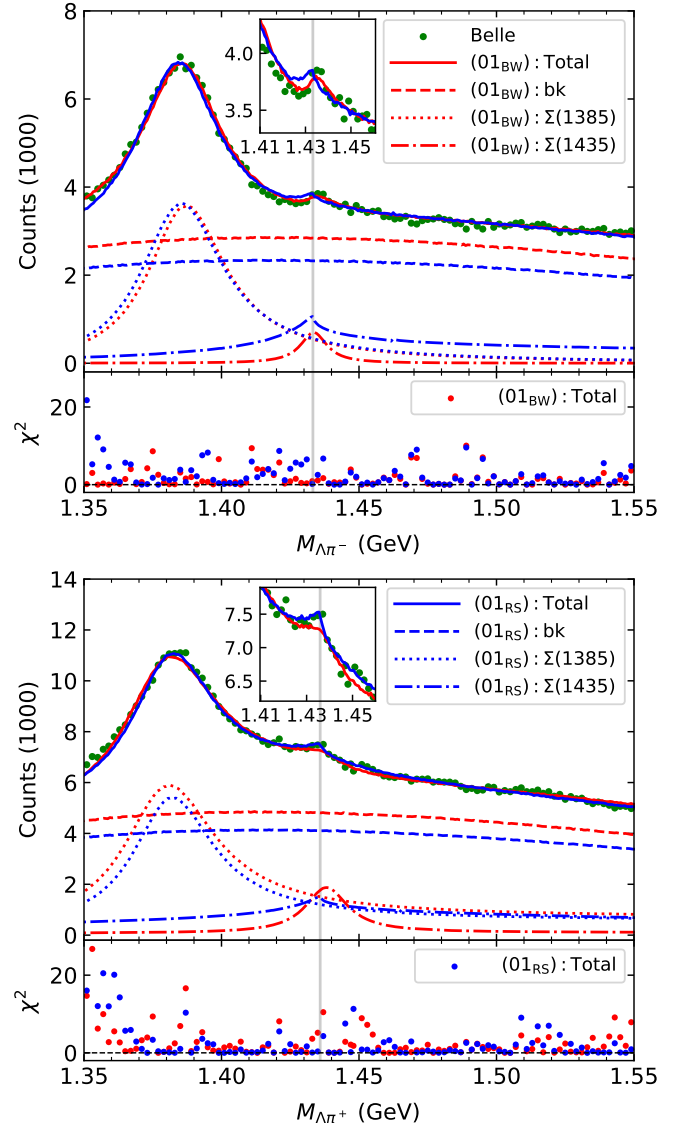


FIG. 3: Invariant mass spectra of $\Lambda\pi^-$ (upper panel) and $\Lambda\pi^+$ (lower panel) with the inclusion of the $\Sigma(1435)$ resonance. The curves correspond to two fitting scenarios: (01_{BW}) , where the $\Sigma(1435)$ is modeled as a Breit-Wigner resonance (red), and (01_{RS}) , where the $\Sigma(1435)$ arises from a rescattering mechanism (blue). In each case, the solid, dashed, dotted, and dash-dotted lines represent the total, background, $\Sigma(1385)$, and $\Sigma(1435)$ contributions, respectively. For visibility, the $\Sigma(1435)$ contribution in the $\Lambda\pi^-$ invariant mass spectrum (upper panel) is scaled by a factor of 100. The insets in both the upper and lower panels show a magnified view of the region around 1435 MeV. Experimental data are taken from the Belle Collaboration [27]. The vertical grey lines indicate the K^-n and \bar{K}^0p thresholds. The scatter points at the bottom of each panel show the χ^2 values for individual data points. Legends apply to both panels.

into individual components reveals notable differences. In both cases, the background contributes significantly across the entire energy range and becomes dominant at higher invariant masses, with a larger contribution observed in fit (01_{BW}) . At lower energies, the $\Sigma(1385)$ dominates the spectrum, and its

contribution is comparable between the two scenarios.

The $\Sigma(1435)$ structure appears around 1435 MeV as expected, either as a resonance or through rescattering. Its contribution is substantially more pronounced in the rescattering scenario than in the Breit-Wigner case. In fact, in the Breit-Wigner fit, the direct contribution from the $\Sigma(1435)$ is relatively small and has been scaled by a factor of 100 for visibility. Unlike the Breit-Wigner component, which is sharply localized near 1435 MeV, the rescattering contribution spans a broader energy range and effectively compensates for the reduced background in fit (01_{RS}). Interestingly, although the direct Breit-Wigner amplitude is minimal, it still induces a noticeable enhancement in the total event yield near 1435 MeV, primarily due to interference effects with other components.

Furthermore, the rescattering mechanism generates a clear cusp precisely at the K^-n and \bar{K}^0p thresholds, whereas the peak of the Breit-Wigner resonance lies slightly above these thresholds. As shown in the inset of Fig. 3, the $\Lambda\pi^+$ invariant mass spectrum measured by Belle exhibits a distinct cusp-like structure, which strongly favors the rescattering interpretation—especially in light of the sharp drop observed at the threshold. In contrast, the $\Lambda\pi^-$ spectrum shows no evident cusp behavior.

It is also worth noting that, unlike the Belle analysis, where separate cusp parameters were introduced independently for the two charge states, the present study incorporates an explicit interaction mechanism that predicts a common cusp shape for both the $\Lambda\pi^+$ and $\Lambda\pi^-$ channels. This constraint results in a poorer fit to the $\Lambda\pi^-$ spectrum compared to the Belle fit and the Breit-Wigner scenario (01_{BW}).

D. Role of $\Sigma(1380)$

Although the $\Lambda\pi^\pm$ invariant mass spectra are generally well reproduced with the inclusion of the $\Sigma(1435)$, noticeable discrepancies remain in the low-energy region, particularly in the $\Lambda\pi^+$ spectrum. In this region, the existence of a $\Sigma(1380)$ state has been proposed in the literature. Previous studies have demonstrated that the combined inclusion of the $\Sigma(1380)$ and $\Sigma(1385)$ is essential to account for the near-threshold enhancement observed in the $p\bar{K}^0$ invariant mass spectrum of the $\Lambda_c^+ \rightarrow p\bar{K}^0\eta$ decay. Motivated by these findings, the present analysis explores the potential impact of the $\Sigma(1380)$ by incorporating it into fits (11_{BW}) and (11_{RS}). Since the $\Sigma(1380)$ does not generate a pronounced structure in the invariant mass distributions, it is modeled as a Breit-Wigner resonance for simplicity in both cases.

With the inclusion of the $\Sigma(1380)$, the fitting in the low-energy region is significantly improved, as the χ^2 for the data points shown in Fig. 3 decreases substantially. It can be observed that the χ^2 values in the low-energy region for both $\Lambda\pi^-$ and $\Lambda\pi^+$ invariant mass spectra are almost zero, as shown in Fig. 4. This improvement is observed in both fittings with $\Sigma(1435)$ as a Breit-Wigner resonance and as rescattering. For the former, the total χ^2 decreases from 418 to 309, while for the latter, it drops from 451 to 291.

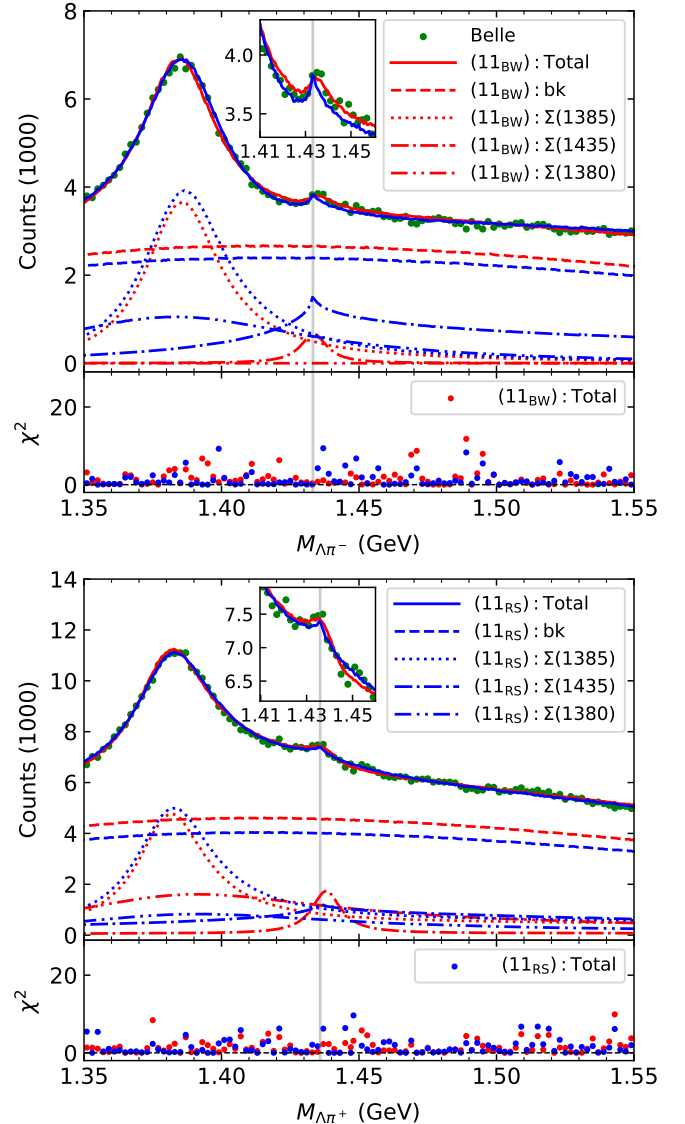


FIG. 4: Invariant mass spectra of $\Lambda\pi^-$ (upper panel) and $\Lambda\pi^+$ (lower panel) with the inclusion of both the $\Sigma(1380)$ and $\Sigma(1435)$ resonances. The curves correspond to two fitting scenarios: (11_{BW}), where the $\Sigma(1435)$ is modeled as a Breit-Wigner resonance (red), and (01_{RS}), where the $\Sigma(1435)$ is dynamically generated via rescattering (blue). In each case, the solid, dashed, dotted, dash-dotted, and dash-dot-dotted curves represent the total, background, $\Sigma(1385)$, $\Sigma(1435)$, and $\Sigma(1380)$ contributions, respectively. For visibility, the $\Sigma(1435)$ contribution in the $\Lambda\pi^-$ invariant mass spectrum (upper panel) is scaled by a factor of 100, and the $\Sigma(1380)$ contributions in both panels are scaled by a factor of 10. Insets in both panels provide a magnified view of the region around 1435 MeV. The experimental data are taken from the Belle Collaboration [27]. Vertical grey lines indicate the K^-n and \bar{K}^0p thresholds. The scatter points at the bottom of each panel represent the χ^2 contributions from individual data points. Legends apply to both panels.

The explicit contributions are also presented in Fig. 4. The background contributions are similar to those without the $\Sigma(1380)$, though the fitting (11_{BW}) has a slightly larger back-

ground contribution compared to (11_{RS}). Combined with the background, the contribution from $\Sigma(1385)$ remains dominant in the lower-energy region. However, the contributions from $\Sigma(1380)$ differ between the Breit-Wigner and rescattering fittings. In the (11_{BW}) fitting, the $\Sigma(1380)$ plays a negligible role in the $\Lambda\pi^-$ spectrum but has a significant impact in the lower-energy region of the $\Lambda\pi^+$ spectrum. In contrast, in the (11_{RS}) fitting, the $\Sigma(1380)$ plays an important role in both spectra, with a larger contribution in the $\Lambda\pi^-$ spectrum. The contributions from $\Sigma(1435)$ as a Breit-Wigner resonance and as rescattering are similar to those without the $\Sigma(1380)$, but the total fit for the structure around 1435 MeV is clearly improved.

In the $\Lambda\pi^-$ spectrum, both scenarios for $\Sigma(1435)$ can produce the dip before the peak, which is not reproduced in the rescattering case without $\Sigma(1380)$. This improvement is attributed to the interference between $\Sigma(1380)$ and rescattering contributions. However, the threshold for K^-n is slightly lower than the experimental peak, making the fit with rescattering slightly worse than the Breit-Wigner resonance. For the $\Lambda\pi^+$ spectrum, both models provide a good fit, with the Breit-Wigner resonance fitting further improved by the inclusion of the $\Sigma(1380)$.

Figure 5 shows a Dalitz-like plot corresponding to the fit (11_{BW}), provided here for reference. A similar distribution is obtained for the fit (11_{RS}). It can be observed that two strips are clearly parallel to the vertical and horizontal axes for the $\Lambda\pi^+$ and $\Lambda\pi^-$ invariant mass spectra, corresponding to the $\Sigma(1385)$ and the interference with $\Sigma(1380)$. Additionally, two dim strips near the main strips represent the contributions from the $\Sigma(1435)$.

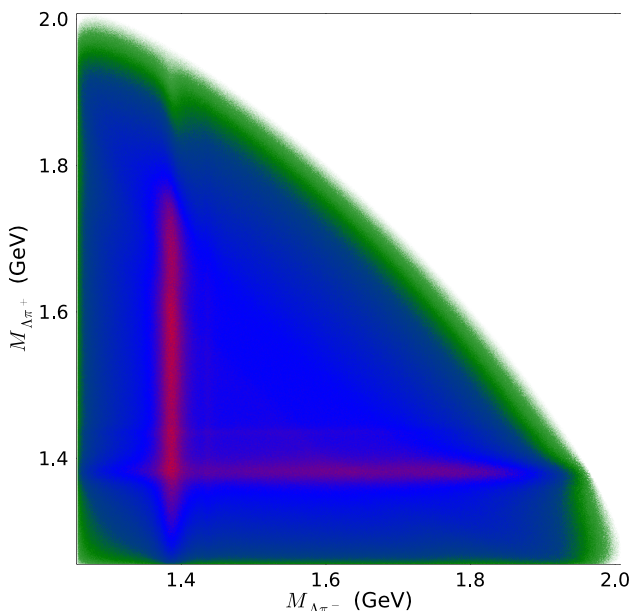


FIG. 5: Dalitz-like plot for $\Lambda_c \rightarrow \Lambda\pi^+\pi^+\pi^-$.

IV. SUMMARY

In this work, the Belle data for the decay process $\Lambda_c \rightarrow \Lambda\pi^+\pi^+\pi^-$ are analyzed using effective Lagrangians, meson-baryon rescattering mechanisms, and the qBSE approach, in combination with event simulations. Simulated events are used to generate the $\Lambda\pi^+$ and $\Lambda\pi^-$ invariant mass spectra, which are subsequently fitted to the experimental data. The model includes contributions from the well-established $\Sigma(1385)$ resonance, two spin-parity $1/2^-$ Σ states—particularly the hypothesized $\Sigma(1380)$ —as well as nonresonant background processes. To describe the structure observed near 1435 MeV, two scenarios are considered: one in which the $\Sigma(1435)$ is modeled as a Breit-Wigner resonance, and another in which it emerges dynamically through coupled-channel rescattering. The combined contributions from these components allow for a satisfactory reproduction of the experimental spectra.

The $\Sigma(1385)$, together with background contributions, provides the dominant contribution in both the $\Lambda\pi^+$ and $\Lambda\pi^-$ spectra. However, to account for the enhancement observed near 1435 MeV, an additional mechanism is necessary. The inclusion of the $\Sigma(1435)$ —either as a Breit-Wigner resonance or through rescattering—helps to describe this structure. While the Breit-Wigner scenario can reproduce the general shape of the enhancement and leads to an improved χ^2 relative to the case without it, the data exhibit a cusp-like feature near the K^-n and \bar{K}^0p thresholds, which is more naturally explained by the rescattering mechanism. This cusp behavior, evident in the $\Lambda\pi^+$ spectrum, supports the interpretation of the $\Sigma(1435)$ as a dynamically generated structure.

Despite these improvements, discrepancies remain in the low-energy region of the $\Lambda\pi^+$ spectrum, which neither the BW nor rescattering scenario alone can fully resolve. To address this, the $\Sigma(1380)$ resonance is included with spin-parity $1/2^-$, as suggested in the literature. Although this state does not manifest as a distinct peak in the invariant mass spectra, its inclusion as a broad Breit-Wigner resonance significantly improves the description of the low-energy region and enhances the fit quality near 1435 MeV as well. Consequently, the combined inclusion of the $\Sigma(1380)$ and $\Sigma(1435)$ leads to a markedly improved agreement with the experimental data.

To quantitatively assess the importance of the intermediate states, their statistical significance is evaluated based on the χ^2 values presented in Table I. Specifically, comparisons are made between the full model and variants excluding either the $\Sigma(1435)$ or $\Sigma(1380)$ resonances. The resulting significance values under both scenarios are summarized in Table II. In all cases, both the $\Sigma(1435)$ and $\Sigma(1380)$ exhibit high statistical significance, indicating their essential roles in accurately reproducing the experimental spectra. The significance of the $\Sigma(1435)$ is comparable between the two scenarios, while the $\Sigma(1380)$ demonstrates slightly higher significance in the rescattering scenario, suggesting that its contribution becomes more critical when the $\Sigma(1435)$ is modeled as a dynamically generated state.

In conclusion, the combined contributions from the $\Sigma(1385)$ and $\Sigma(1435)$, treated both as a Breit-Wigner resonance and via

TABLE II: Statistical significance of the $\Sigma(1435)$ and $\Sigma(1380)$ contributions in the fits under two scenarios: treating the $\Sigma(1435)$ as a Breit-Wigner (BW) resonance or as a rescattering (RS) effect.

$\frac{\Sigma^*}{\text{scenario}}$	$\frac{\Sigma(1435)}{\text{BW}}$	$\frac{\Sigma(1380)}{\text{BW}}$	$\frac{\Sigma(1435)}{\text{RS}}$	$\frac{\Sigma(1380)}{\text{RS}}$
Significance (σ)	13.0	9.7	14.2	12.0

rescattering, and the $\Sigma(1380)$ resonance provide an effective description of the $\Lambda_c \rightarrow \Lambda\pi^+\pi^-\pi^-$ decay process. This

comprehensive model yields a more accurate reproduction of the full experimental invariant mass spectra and highlights the essential role of interference effects among the resonances in describing the observed data.

Acknowledgement I would like to thank Professor Kiyoshi Tanida for kindly explaining the uncertainties of the data and the statistical significance. This project is supported by the National Natural Science Foundation of China (Grant No. 12475080)

- [1] S. Navas *et al.* [Particle Data Group], “Review of particle physics,” Phys. Rev. D **110**, no.3, 030001 (2024)
- [2] S. Capstick and N. Isgur, “Baryons in a relativized quark model with chromodynamics,” Phys. Rev. D **34**, no.9, 2809-2835 (1986)
- [3] A. V. Sarantsev, M. Matveev, V. A. Nikonov, A. V. Anisovich, U. Thoma and E. Klempt, “Hyperon II: Properties of excited hyperons,” Eur. Phys. J. A **55**, no.10, 180 (2019)
- [4] J. A. Oller and U. G. Meissner, “Chiral dynamics in the presence of bound states: Kaon nucleon interactions revisited,” Phys. Lett. B **500**, 263-272 (2001)
- [5] D. Jido, J. A. Oller, E. Oset, A. Ramos and U. G. Meissner, “Chiral dynamics of the two Lambda(1405) states,” Nucl. Phys. A **725**, 181-200 (2003)
- [6] A. Zhang, Y. R. Liu, P. Z. Huang, W. Z. Deng, X. L. Chen and S. L. Zhu, “ $J^P = 1/2^-$ pentaquarks in Jaffe and Wilczek’s diquark model,” HEPNP **29**, 250 (2005)
- [7] J. J. Wu, S. Dulat and B. S. Zou, “Evidence for a new Σ^* resonance with $J^P = 1/2^-$ in the old data of $K^-p \rightarrow \Lambda\pi^+\pi^-$ reaction,” Phys. Rev. D **80**, 017503 (2009)
- [8] D. O. Huwe, “Study of the reaction $K^- + p \rightarrow \Lambda + \pi^+ + \pi^-$ from 1.2 to 1.7 bev/c,” Phys. Rev. **181**, 1824-1853 (1969)
- [9] J. J. Wu, S. Dulat and B. S. Zou, “Further evidence for the Σ^* resonance with $J^P = 1/2^-$ around 1380 MeV,” Phys. Rev. C **81**, 045210 (2010)
- [10] J. J. Xie, J. J. Wu and B. S. Zou, “Role of the possible $\Sigma^*(\frac{1}{2}^-)$ state in the $\Lambda p \rightarrow \Lambda p \pi^0$ reaction,” Phys. Rev. C **90**, no.5, 055204 (2014)
- [11] Y. H. Chen and B. S. Zou, “Possible $\Sigma^*(1/2^-)$ in the initial-state polarized $\gamma N \rightarrow K^+\Sigma^*(1385) \rightarrow K^+\pi\Lambda$ reaction near threshold,” Phys. Rev. C **88**, no.2, 024304 (2013)
- [12] L. Roca and E. Oset, “ $\Lambda(1405)$ poles obtained from $\pi^0\Sigma^0$ photoproduction data,” Phys. Rev. C **87**, no.5, 055201 (2013)
- [13] P. Gao, J. J. Wu and B. S. Zou, “Possible $\Sigma(\frac{1}{2}^-)$ under the $\Sigma^*(1385)$ peak in $K\Sigma^*$ photoproduction,” Phys. Rev. C **81**, 055203 (2010)
- [14] G. Y. Wang, N. C. Wei, H. M. Yang, E. Wang, L. S. Geng and J. J. Xie, “Roles of $a_0(980)$, $\Lambda(1670)$, and $\Sigma(1385)$ in the $\Lambda_c \rightarrow \eta\Lambda\pi^+$ decay,” Phys. Rev. D **106**, no.5, 056001 (2022)
- [15] W. T. Lyu, S. C. Zhang, G. Y. Wang, J. J. Wu, E. Wang, L. S. Geng and J. J. Xie, “Evidence of the low-lying baryon $\Sigma^*(1/2^-)$ in the process $\Lambda_c^+ \rightarrow \eta\pi^+\Lambda$,” Phys. Rev. D **110**, no.5, 054020 (2024)
- [16] Y. Li, S. W. Liu, E. Wang, D. M. Li, L. S. Geng and J. J. Xie, “Theoretical study of $N(1535)$ and $\Sigma^*(1/2^-)$ in the Cabibbo-favored process $\Lambda_c^+ \rightarrow pK^0\eta$,” Phys. Rev. D **110**, no.7, 074010 (2024)
- [17] R. Pavao, S. Sakai and E. Oset, “Production of $N^*(1535)$ and $N^*(1650)$ in $\Lambda_c \rightarrow \bar{K}^0\eta p$ (πN) decay,” Phys. Rev. C **98**, no.1, 015201 (2018)
- [18] E. Oset and A. Ramos, “Nonperturbative chiral approach to s wave $\bar{K}N$ interactions,” Nucl. Phys. A **635**, 99-120 (1998)
- [19] M. Mai and U. G. Meißner, “Constraints on the chiral unitary $\bar{K}N$ amplitude from $\pi\Sigma K^+$ photoproduction data,” Eur. Phys. J. A **51**, no.3, 30 (2015)
- [20] M. Mai, “Review of the $\Lambda(1405)$ A curious case of a strangeness resonance,” Eur. Phys. J. ST **230**, no.6, 1593-1607 (2021)
- [21] D. Sadasivan, M. Mai, M. Döring, U. G. Meißner, F. Amorim, J. P. Klucik, J. X. Lu and L. S. Geng, “New insights into the pole parameters of the $\Lambda(1380)$, the $\Lambda(1405)$ and the $\Sigma(1385)$,” Front. Phys. **11**, 1139236 (2023)
- [22] E. Wang, L. S. Geng, J. J. Wu, J. J. Xie and B. S. Zou, “Review of the Low-Lying Excited Baryons $\Sigma^*(1/2^-)$,” Chin. Phys. Lett. **41**, no.10, 101401 (2024)
- [23] K. P. Khemchandani, A. Martínez Torres and J. A. Oller, “Hyperon resonances coupled to pseudoscalar- and vector-baryon channels,” Phys. Rev. C **100**, no.1, 015208 (2019)
- [24] L. Roca and E. Oset, “Isospin 0 and 1 resonances from $\pi\Sigma$ photoproduction data,” Phys. Rev. C **88**, no.5, 055206 (2013)
- [25] K. Moriya *et al.* [CLAS], “Measurement of the $\Sigma\pi$ photoproduction line shapes near the $\Lambda(1405)$,” Phys. Rev. C **87**, no.3, 035206 (2013)
- [26] J. J. Xie and E. Oset, “Search for the Σ^* state in $\Lambda_c^+ \rightarrow \pi^+\pi^0\pi^-\Sigma^+$ decay by triangle singularity,” Phys. Lett. B **792**, 450-453 (2019)
- [27] Y. Ma *et al.* [Belle], “First Observation of $\Lambda\pi^+$ and $\Lambda\pi^-$ Signals near the $\bar{K}N(I=1)$ Mass Threshold in $\Lambda_c^+ \rightarrow \Lambda\pi^+\pi^-\pi^-$ Decay,” Phys. Rev. Lett. **130**, no.15, 151903 (2023)
- [28] F. James, “Monte-Carlo phase space,” CERN-68-15 (1968)
- [29] <https://github.com/junhe1979/DalitzPlot.jl>
- [30] J. K. Ahn, S. Yang and S. I. Nam, “Hyperon production in $\Lambda_c^+ \rightarrow K^-p\pi^+$ and $\Lambda_c^+ \rightarrow K_S^0 p\pi^0$,” Phys. Rev. D **100**, no.3, 034027 (2019)
- [31] Z. Y. Wang, S. Q. Luo, Z. F. Sun, C. W. Xiao and X. Liu, “Study of the resonance contributions in the $\Xi_b^- \rightarrow pK^-K^-$ decay,” Phys. Rev. D **106**, no.9, 096026 (2022)
- [32] S. Y. Kong, J. T. Zhu, S. Chen and J. He, “Production of open-charm pentaquark molecules in decay $B^0 \rightarrow \bar{D}^0 p\bar{p}$,” Phys. Rev. D **110**, no.9, 9 (2024)
- [33] J. He and P. L. Lu, “The octet meson and octet baryon interaction with strangeness and the $\Lambda(1405)$,” Int. J. Mod. Phys. E **24**, no.11, 1550088 (2015)
- [34] J. He, “Study of the $B\bar{B}^*/D\bar{D}^*$ bound states in a Bethe-Salpeter

- approach,” Phys. Rev. D **90**, no.7, 076008 (2014)
- [35] J. He, “The $Z_c(3900)$ as a resonance from the $D\bar{D}^*$ interaction,” Phys. Rev. D **92**, no.3, 034004 (2015)
- [36] J. He and D. Y. Chen, “ $Z_c(3900)/Z_c(3885)$ as a virtual state from $\pi J/\psi - \bar{D}^*D$ interaction,” Eur. Phys. J. C **78**, no.2, 94 (2018)
- [37] J. He, “Internal structures of the nucleon resonances N(1875) and N(2120),” Phys. Rev. C **91**, no.1, 018201 (2015)
- [38] J. He, “ $\bar{D}\Sigma_c^*$ and $\bar{D}^*\Sigma_c$ interactions and the LHCb hidden-charmed pentaquarks,” Phys. Lett. B **753**, 547-551 (2016)
- [39] F. Gross, “Charge conjugation invariance of the spectator equations,” Few Body Syst. **30**, 21-29 (2001)
- [40] L. J. Liu, E. Wang, J. J. Xie, K. L. Song and J. Y. Zhu, “ $\Lambda(1405)$ production in the process $\chi_{c0}(1P) \rightarrow \bar{\Lambda}\Sigma\pi$,” Phys. Rev. D **98**, no.11, 114017 (2018)